



Experimental demonstration of rainbow trapping of elastic waves in two-dimensional axisymmetric phononic crystal plates^{a)}

Chadi Ellouzi,¹ Ali Zabihi,¹ Louis Gormley,¹ Farhood Aghdasi,¹ Katerina Stojanoska,¹ Amir Miri,² Datneshwar Jha,¹ Dand Chen Shen^{1,b)}

ABSTRACT:

Structures with specific graded geometries or properties can cause spatial separation and local field enhancement of wave energy. This phenomenon is called rainbow trapping, which manifests itself as stopping the propagation of waves at different locations according to their frequencies. In acoustics, most research on rainbow trapping has focused on wave propagation in one dimension. This research examined the elastic wave trapping performance of a two-dimensional (2D) axisymmetric grooved phononic crystal plate structure. The performance of the proposed structure is validated using numerical simulations based on finite element analysis and experimental measurements using a laser Doppler vibrometer. It is found that rainbow trapping within the frequency range of 165–205 kHz is achieved, where elastic waves are trapped at different radial distances in the plate. The results demonstrate that the proposed design is capable of effectively capturing elastic waves across a broad frequency range of interest. This concept could be useful in applications such as filtering and energy harvesting by concentrating wave energy at different locations in the structure. © 2024 Acoustical Society of America. https://doi.org/10.1121/10.0025179

(Received 5 September 2023; revised 30 January 2024; accepted 20 February 2024; published online 4 March 2024)

[Editor: Vladislav Sergeevich Sorokin] Pages: 1759–1766

I. INTRODUCTION

In recent years, frequency-selective structures have become increasingly important in many engineering fields due to their ability to act as passive filters for different types of waves. These structures possess a variety of interesting attributes. For example, they can improve acoustic wave sensing, filtering, and sound energy absorption, ^{1–7} as well as isolate desired frequencies in the multimodal-Lamb wave, which makes structural health monitoring of thin plates more efficient. ^{8–10} Among the many potential applications for these structures, a unique phenomenon is the rainbow trapping effect. ^{11–17} This effect has been demonstrated to filter waves both spatially and spectrally ^{18–22} and was initially applied to electromagnetic waves to control optical delays and to temporarily store light, ^{23–25} but has since been applied to acoustic waves as well.

Several studies have investigated the phenomenon of acoustic rainbow trapping, such as Tian and Yu, ²⁸ who used a wafer-type piezoelectric actuator to investigate the rainbow trapping of ultrasonic guided waves in a one-dimensional (1D) chirped phononic crystal plate in the frequency range of 130–180 kHz. The COMSOL simulation results were validated with a scanning laser Doppler vibrometer (LDV), confirming the gradual reduction in group

velocity along the structure. Arreola-Lucas *et al.*²⁹ experimentally examined the mechanical analog of rainbow trapping in 1D elastic systems. More examples can be found in graded phononic crystals and metamaterials that exhibit gradient effective properties for frequency-dependent manipulation of wave energy.³⁰

Other studies used microphones and speakers to capture guided waves. They were able to create the mechanical equivalent of the rainbow trapping effect in the lowfrequency range of 200-500 Hz by using a speaker to excite a single monopolar Mie resonance.³¹ Furthermore, inspiration from the coiled shape of the cochlear rainbow trapping effect was studied in the frequency range of 1-10 kHz by producing sound waves using a small loudspeaker, based on measurements obtained from a LDV. 32 In other research, an electrodynamic shaker was used to excite the waveguide, and three-dimensional (3D) LDV was employed to record flexural waves that were captured by a range of resonators with varying lengths.³³ Additionally, other studies have attempted to advance the frequency trapping concept by combining multiple methods, which enhances the system's efficiency. For instance, a programmable piezoelectric metamaterial beam containing a graded array of piezoelectric unit cells connected to synthetic impedance circuits was used to create a programmable rainbow trapping. Additionally, the graded array of resonators embedded in a host structure was used to manipulate wave propagation by capitalizing on the resonator-structure interaction, thereby

¹Department of Mechanical Engineering, Rowan University, Glassboro, New Jersey 08028, USA

²Department of Biomedical Engineering, New Jersey Institute of Technology, Newark, New Jersey 07102, USA

a)This paper is part of the special issue on Wave Phenomena in Periodic, Near-Periodic, and Locally Resonant Systems.

b)Email: shenc@rowan.edu

creating wave confinement.³⁴ In recent years, researchers have also started to combine the concept of rainbow trapping and topological insulators. Energy trapping with robust wave propagation characteristics immune to defects or disorders in the structures has been realized.^{35–37} Furthermore, a variety of studies have begun to empirically illustrate the theory of rainbow trapping in other wave forms. These include spoof surface plasmon polaritons,³⁸ phononics and acoustics,³⁹ water waves,^{40,41} and fluid-loaded elastic plates.⁴²

Achieving rainbow trapping could open several profound applications. For example, broadband energy harvesting devices may be realized by localizing and concentrating wave energy at different sites. However, most of the existing research on the rainbow trapping of elastic waves is based on unidimensional linear phononic crystal structures. This limits the applicability of these devices as elastic waves in thin plates, shells, or engineering structures usually propagate along multiple directions. Expanding the rainbow trapping effect into two dimensions can further improve its performance in real structures and bridge the gap in its real-world applications.

In this paper, we study the acoustic rainbow trapping performance of a two-dimensional (2D) axisymmetric phononic crystal structure. A 1D graded phononic crystal is first designed, and the structure is extended into 2D axisymmetric structures for the rainbow trapping of elastic waves in two dimensions. The performance was assessed both numerically and experimentally using finite element analysis and laser vibrometer-based measurements. The results showed that the proposed 2D axisymmetric phononic crystal design is capable of effectively trapping elastic waves over a wide range of frequencies. This concept could be beneficial for many engineering applications, such as energy harvesting and noise suppression applications.

II. STRUCTURAL DESIGN

To begin with, we designed a 2D axisymmetric phononic crystal plate structure out of a 3.2 mm thick aluminum plate. It incorporates an array of 34 equally wide grooves that measure 2.7 mm in width (w) and 1.27 mm in depth (d). The overall diameter (D) of the structure is 452 mm.

This plate was used to spatially modulate the stop band and group velocity of ultrasonic guided waves to create a rainbow trapping effect. Figures 1(a)-1(c) illustrate the overall structure, the cross section of the plate, and three consecutive cells: n-1, n, and n+1, respectively. The extrusion width, E_w , increases from 2 mm to 3.65 mm along the x direction of the plate at an interval of $\varepsilon = 0.05$ mm. In the proposed grooved phononic crystal plate, the length of each cell increases linearly along the x direction. Since the difference between two adjacent cells is very small, the structure can be studied by the quasi-periodic nature of the unit cells. Thus, we can use the frequency-wavenumber dispersion relation f(k). This is derived by numerically solving a modal analysis problem on a unit cell with

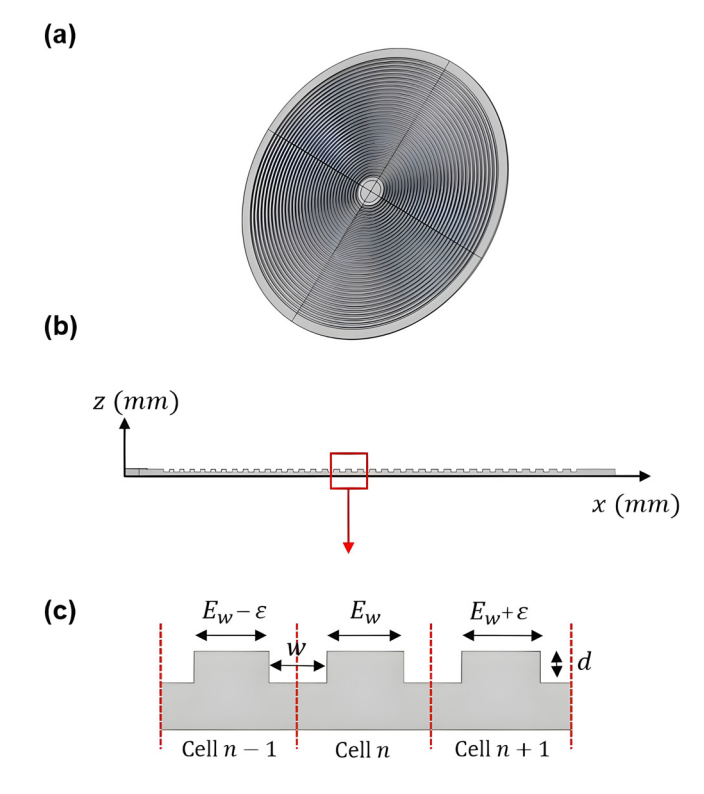


FIG. 1. (Color online) Schematics of the 2D grooved axisymmetric phononic crystal plate. (a) 3D view of the proposed structure. (b) Cross-sectional view of the plate. (c) Illustration of three consecutive cells in the plate and the associated dimensions.

Bloch-Floquet boundary condition to approximate the dispersion characteristics at the nth cell in the grooved phononic crystal plate. Since 2D wave propagation is involved, the amplitude of the waves will naturally decay when they travel along the radial direction. In practice, such a condition can be difficult to model using the Bloch theorem, and sometimes a modified design needs to be carried out so that periodicity is enforced. 43,44 For simple radially periodic plates, a closed-form analytic solution may exist, 45 however, the structural configuration of the phononic crystal plate is complex, and hence its band structure is obtained from numerical simulations based on finite element analysis. To simplify the definitions in the numerical setup so that all the calculations are still carried out in the Cartesian coordinate system, an effective decay rate denoted as γ is established to ensure energy conservation across the boundaries of the two adjacent unit cells, as described by the subsequent equation. 45,46

$$\vec{u}_2 = \vec{u}_1 e^{ik(1+\gamma)},\tag{1}$$

where \vec{u}_1 , \vec{u}_2 are the displacement vectors at the boundaries of the unit cell and k is the wave vector. The cell length in the chirped phononic crystal plate increases in a linear fashion as it moves along the x direction, leading to different decay rates along the radial direction. As a result, the unit cells at various radial distances along the plate will have different frequency-wavenumber dispersion curves.

To demonstrate the spatial evolution of these curves, Figs. 2(a)–2(c) depict the frequency-wavenumber dispersion curves by numerical simulations using COMSOL MULTIPHYSICS in the first Brillouin zone for cells located at three different points: x=14 mm (the first cell with length $L_1=2$ mm), x=95.2 mm (the 17th cell with length $L_{17}=2.8$ mm), and x=195.5 mm (the 34th cell with length $L_{34}=3.65$ mm). The following parameters are used in the simulations for the aluminum plate: density: $\rho=2700$ kg/ m^3 , Young's modulus E=68.9 GPa, and Poisson's ratio v=0.33. Within the frequency range shown in Figs. 2(a)–(c), there are two types of stop bands.

The first stop band, known as the Bragg stop band, is located at point A on the boundary of the first Brillouin zone. This stop band is created by the Bragg reflection of the A0 mode, which disrupts the dispersion curve of the A0 asymmetric mode and stops it from traveling. The second stop band, the full stop band marked by B in the figures, is the S0-A0 stop band caused by the coupling between the symmetric S0 and asymmetric A0 modes. Clearly, as the extrusion width increases, the full stop band shifts to the lower frequency range, while other main characteristics of the band structure are maintained. Figure 2(d) shows how the stop band frequency changes, depending on the position along the *x* axis in the grooved phononic crystal plate with and without natural decay. As the *x*-location increases, the

width of the stop band gets slightly smaller and the stop band moves to lower frequencies. Hence, if guided waves that carry frequencies in the range 165 to \sim 205 kHz come into the phononic crystal plate from the first cell and move in the positive x-direction, different frequency components will arrive at locations that are on the lower edge of the stop band. At these places, the waves will stop moving forward.

It should be noted that the stop band frequency shows a subtle variance when a natural decay is considered, as opposed to when there is no decay. The most significant discrepancy is observed at the initial few unit cells, diminishing towards the disk's periphery. This pattern can be attributed to the conservation of energy across both edges of each unit cell, with variations in the effective decay rate γ . The rate γ is related to the proportion between the radius of each unit cell and decreases as one moves outward along the disk's radius. The inner edge of the disk experiences the greatest shift in this rate, primarily because the ratio of radii of two adjacent unit cells is greatest in this region. However, overall, the consideration of the decay does not significantly alter the operational frequency range of the structure. Consequently, employing a simplified rectangular model that disregards the decay can still yield a reasonable performance, as will be shown later.

The results indicate that 1D rainbow trapping can be realized by arranging the unit cells in a graded manner.

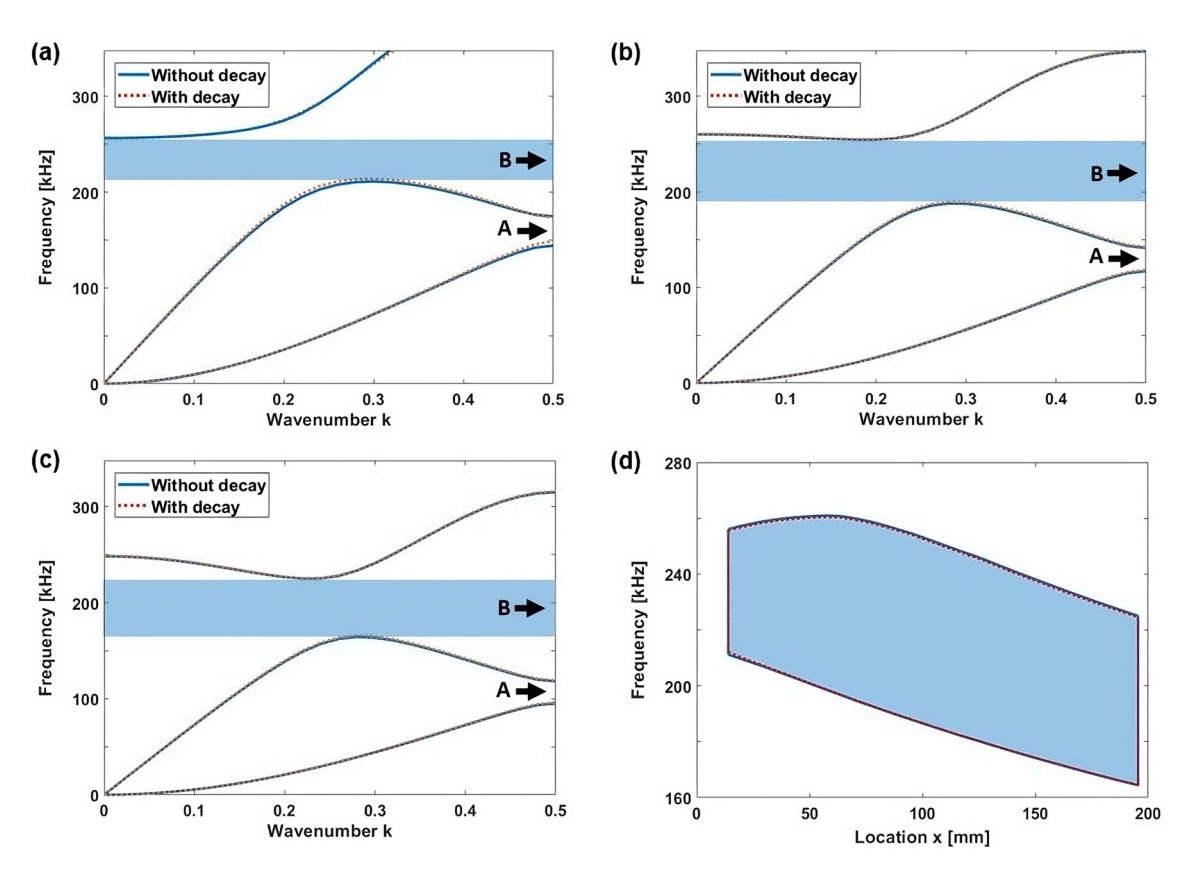


FIG. 2. (Color online) Dispersion analysis. (a)–(c) Local frequency-wavenumber dispersion curves in the first Brillouin zone for the 1st cell (left), 17th cell (center), and 34th cell (right) of the grooved phononic crystal plate, respectively. The solid and dashed curves represent the band structure without and with natural decay along the radial direction. (d) Variation of local stop band with respect to location *x* in the phononic crystal plate. The shaded areas represent stop bands.

Next, the structure is revolved to form the 2D phononic crystal plate. As the structure is axisymmetric, incoming waves generated at the center of the plate will then get trapped at different radial distances based on the symmetry conditions.

III. NUMERICAL SIMULATION

Using COMSOL MULTIPHYSICS, a 3D representation of the multi-grooved disk was created, taking into consideration the 2D axisymmetric nature of the structure during the simulation setup. To this end, frequency-domain analysis was first carried out to examine the frequency response of the phononic crystal plate based on the equation

$$-\rho\omega^2 u = \nabla \cdot \sigma + Fe^{i\phi},\tag{2}$$

where the material density is donated by ρ , the angular frequency is presented by ω , and F stands for the external force, while ϕ presents the phase angle of the applied force and σ is the stress tensor in the structure.

To replicate the vibrations from a piezoelectric transducer, an axial boundary load was applied to the disk's top surface between $r=0\,\mathrm{mm}$ and $r=3.65\,\mathrm{mm}$. Furthermore, to minimize any unwanted reflections that the boundaries might cause, a low-reflection boundary was allocated to the disk's perimeter. Free boundaries were applied to all remaining surfaces to prevent any damping effect that can affect the acoustic trapping simulation results. Five different acoustic excitation frequencies (165, 175, 185, 195, and 205 kHz) were used in the simulation to examine the disk's performance in terms of the acoustic trapping effect within the frequency range of interest (Fig. 3).

The simulation results show that the normalized total displacement caused by the piezoelectric transducer in relation to the disk radius is dependent on the frequency used. At 165 kHz, the sound wave was able to travel through the

entire disk, leading to non-zero displacement fields across the whole disk. On the other hand, at 205 kHz, only the inner part of the disk experienced a significant amount of displacement from the transducer. This decrease in displacement was consistent with the expectation of the acoustic rainbow trapping effect. As the location of the disk radius increased, the group velocities decreased until eventually reaching zero for different frequencies at certain locations.

To confirm the frequency-domain analysis results, a time-domain simulation was also made in conjunction with the previous one. A sinusoidal wave with 20 cycles shown in Fig. 4(a) was used to excite the phononic crystal plate, and the local normal velocity amplitude was recorded at three distinct points across the disk. The initial point was positioned at the first unit cell, located at 14 mm away from the center. The second measurement point was set at the disk's midpoint, 95.2 mm from the center, while the third was at the disk's outer cell, located 195.5 mm from the center. Three different frequencies were studied, namely 165, 185, and 205 kHz, similarly to the process used in the frequency-domain analysis. The corresponding normalized wave amplitudes for each frequency at each point are depicted in Fig. 4. It can be seen that the results from timedomain simulations align with those derived from frequency-domain analyses. Sound waves were able to propagate through the first unit cell for all the three examined frequencies. Meanwhile, at the midpoint of the disk, sound wave propagation was detected only at frequencies of 165 and 185 kHz. At the disk's outer perimeter, sound propagation was exclusively present at a frequency of 165 kHz, while the two other frequencies were greatly suppressed, validating analytical predictions associated with the theory of the rainbow trapping effect. This pattern mirrors that observed in a 1D plate, confirming the ability of the 2D axisymmetric disk to selectively confine elastic waves based on their frequency characteristics.

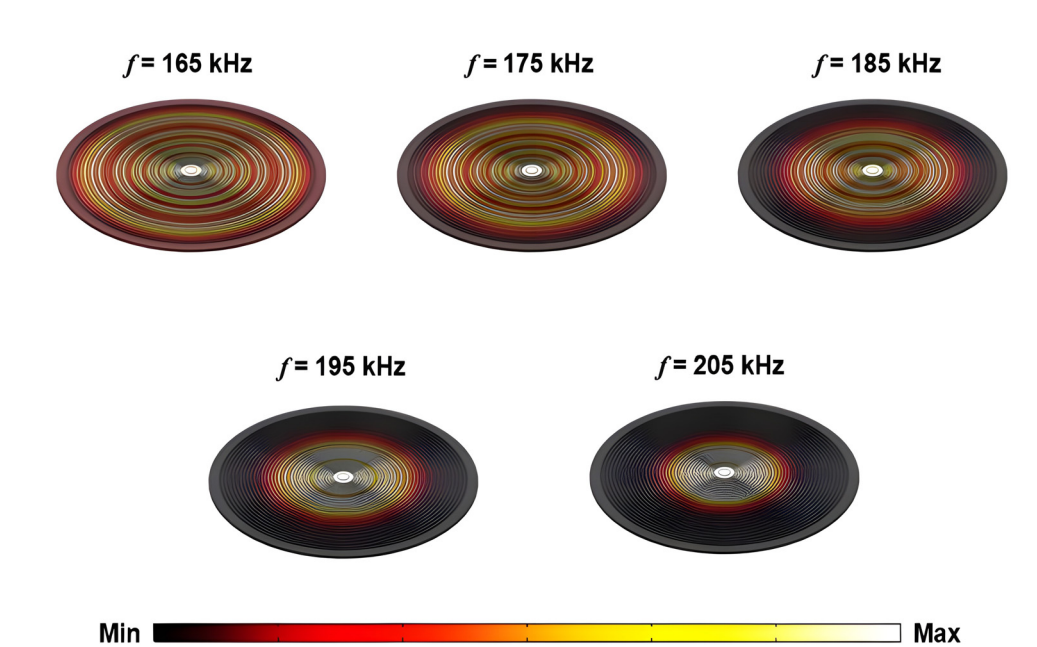


FIG. 3. (Color online) Total displacement field of the 2D axisymmetric grooved discs at different operating frequencies. The waves emitted at the center of the disk stop at different locations according to their frequencies.

https://doi.org/10.1121/10.0025179

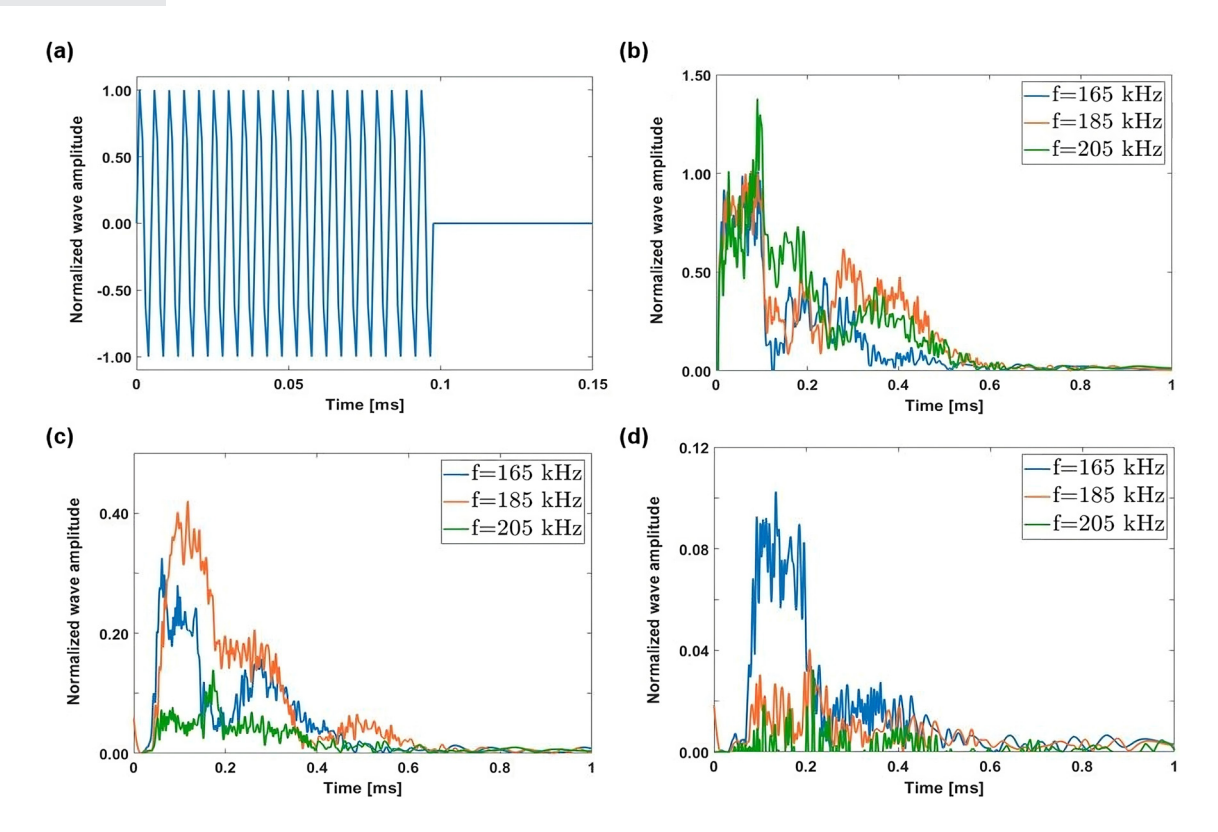


FIG. 4. (Color online) Time-domain simulation of the phononic crystal plate. (a) Single sinusoidal wave input signal. (b), (c), and (d) upper envelope of normalized wave amplitude at the 1st point located at x = 14 mm, 2nd point at x = 95.2 mm, and 3rd point at x = 195.5 mm from the center of the grooved phononic crystal plate, respectively.

IV. EXPERIMENTAL RESULTS

To test the device's performance, a prototype grooved disk was made from 6061-T6 aluminum sheets with a 3.2 mm thickness using a computer numerical control (CNC) machine. A ceramic ring piezoelectric transducer (SMR, Davenport, FL) was glued to the center of the disk, using fast-curing epoxy (J-B Weld, Pemberton, NJ) to provide the necessary acoustic actuation. The transducer and disk were suspended in the air with a custom-made wooden support and hanging strings to avoid any physical contact with other objects to mimic a free boundary condition. A function generator (RIGOL DG4162; Rigol, Portland, OR) was used to combine a sinusoidal burst with a Gaussian envelope to drive the piezoelectric transducer. The input signals were amplified by a radio frequency (RF) amplifier (ENI 3200 L; Bell Electronics NW, Inc., Renton, WA) so that a vibration of sufficient intensity was created within the plate. A digital free beam laser vibrometer (Optomet Nova, Berlin, Germany) was used to measure the disk total displacement at several specific points in the direction of the laser beam. The general experimental setup can be seen in Fig. 5(a).

The sinusoidal burst input wave helps distinguish between the direct-transmitted and reflected signals from the boundaries as they are separated in time. The vibrometer was used to collect the raw experimental data processed through optogui software.

To maintain the measurement signal while eliminating any background noise, a 10 Hz high-pass Butterworth filter

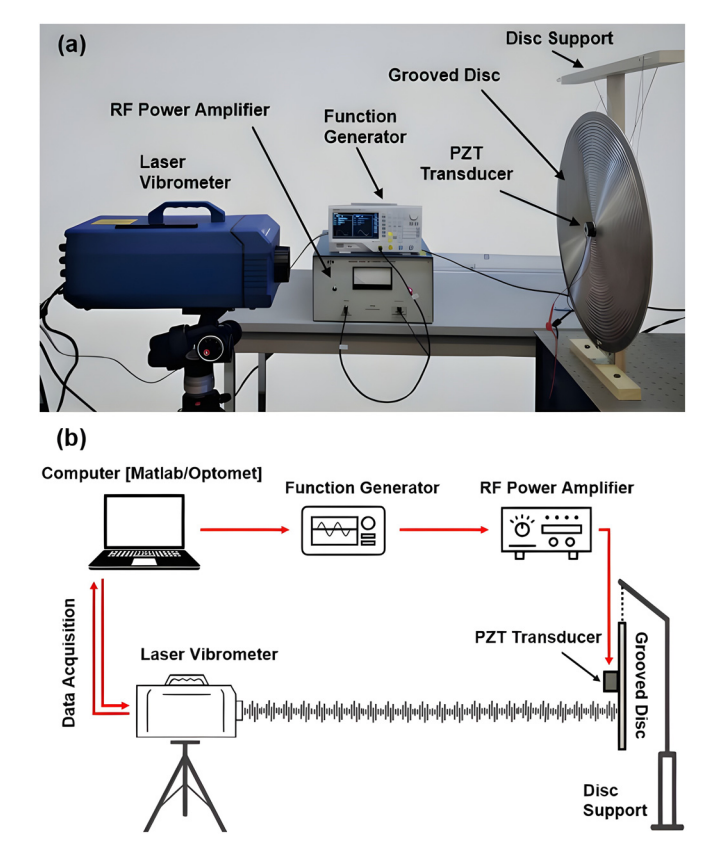


FIG. 5. (Color online) Measurement setup. (a) Photo of the experimental setup. (b) Schematic showing the measurement setup and the process of data acquisition.

was applied. A designated sliding window was further defined to keep the original burst signal intact while setting other signals outside the window, including the unnecessary reflected waves, to zero. Figure 5(b) illustrates the overall process of data acquisition. In the measurement, the displacement data were obtained at 15 points arranged at a consistent 13 mm distance apart along the disk's radial direction for measurement accuracy, with the first point positioned at the center of the first groove, 14 mm from the disk center. A typical measured signal is shown in Fig. 6, where the direct-transmitted and reflected Gaussian pulses are clearly observable.

The filtered frequency response data from the grooved disk were plotted against the simulation results for the selected frequencies in Fig. 7. The experimental and numerical results agree well with each other at all frequencies and follow the same curve tendency. At lower frequencies, the waves propagate further to the outer edge of the edge, and the wave energy is observed at larger radial distances. On the contrary, the wave energy drops quickly after being launched by the actuator. Some slight differences between the experimental and simulation data can be observed due to experimental noise, fabrication imperfections, and non-ideal boundary conditions compared to numerical simulations. The locations where waves stop propagating forward are nearly the same, and the regions with intensive energy agree well with each other. At 165 kHz, the experimental results match the simulation results and spread throughout the radius of the grooved disk. As expected, only the inner part of the disk is impacted at 205 kHz.

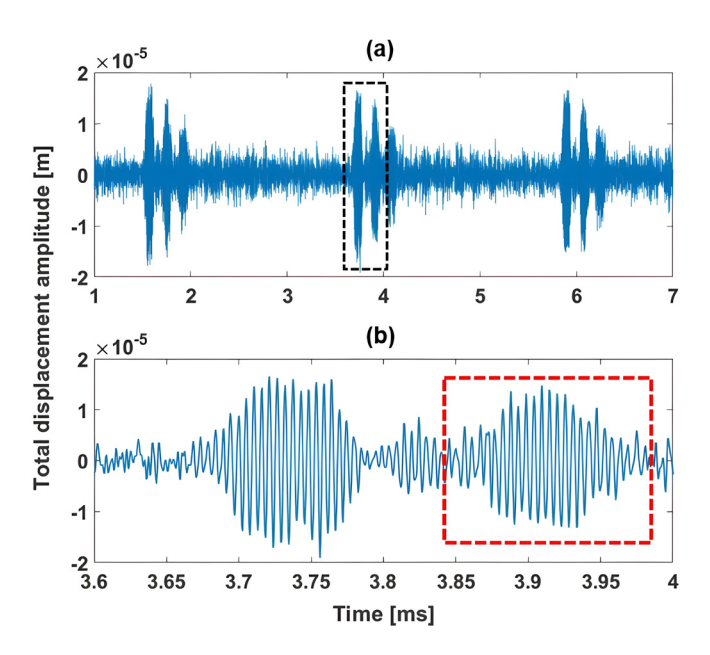


FIG. 6. (Color online) Experimentally obtained raw signals. (a) Time-domain signals show a few cycles of burst signals. (b) Zoomed view of dotted box in the panel. The reflected signals are marked in the red dotted box and are separated from the directly transmitted signals because of their propagation time.

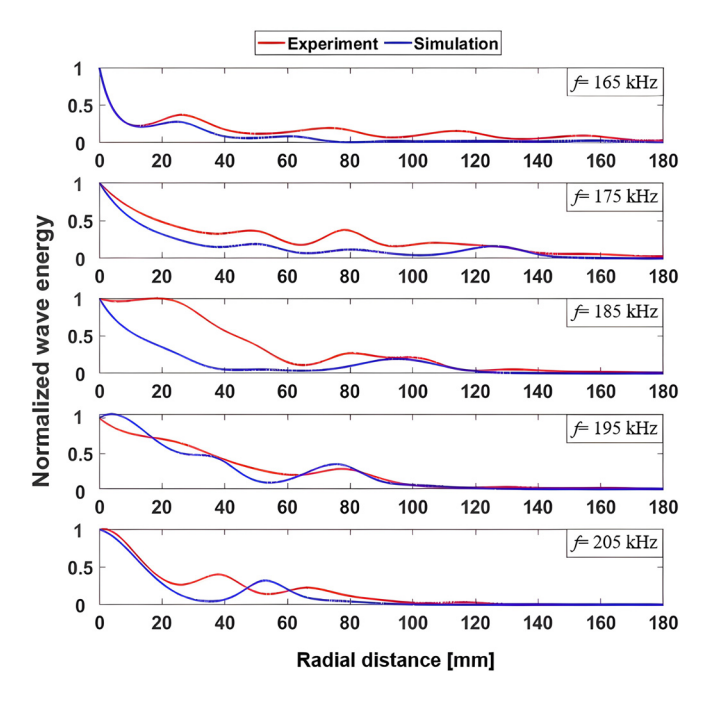


FIG. 7. (Color online) Comparisons between experimental and numerical results at various frequencies.

V. CONCLUSION

This study demonstrated a rainbow trapping effect of ultrasonic waves in 2D axisymmetric grooved discs with spatially variant dispersion, group velocity, and stop band. Through simulation and experiment, we demonstrated rainbow trapping of ultrasonic waves in the frequency range of 165 to \sim 205 kHz. The demonstrated rainbow trapping phenomenon is related to the progressively slowing group velocity in space and the spatially variant dispersion characteristics. As ultrasonic waves travel along the various grooves of the 2D axisymmetric plate, they gradually slow down due to the slowing group velocity. This causes the energy of guided waves to concentrate at the low-velocity area close to the lower boundary of the stop band. Additionally, due to the varying dispersion characteristics, the wave energy of different frequencies can be concentrated at separate locations, producing a rainbow trapping effect. Our work expands elastic wave rainbow trapping into two dimensions, possessing higher relevance to engineering structures. 47,48

With the achieved results and experimental demonstration presented in this study, the ultrasonic field will be enlightened for potential interesting work related to 2D ultrasonic guided waves through the ultrasonic rainbow trapping effect. The proposed approach can be useful for many different applications. For example, by focusing wave energy based on its frequency, various piezoelectric components can be placed in areas to maximize output power. Another potential application can be found in the field of acoustofluidics, where particles with varying sizes and attributes can be concentrated using distinct trapped frequencies, ⁴⁹ providing a new way to separate biological samples based on their population.

ACKNOWLEDGMENTS

This work was supported by the National Science Foundation (NSF) (CMMI-2137749 and CBET-2243507) and a grant from the New Jersey Economic Development Authority. C.E. and A.Z. contributed equally to this work.

AUTHOR DECLARATIONSConflict of Interest

The authors have no conflicts to declare.

DATA AVAILABILITY

The data that support the findings of this study are available from the corresponding author upon reasonable request.

- ¹K. A. Rashid, B. Li, and Z. Shen, "An overview of three-dimensional frequency-selective structures," IEEE Antennas Propag. Mag. **56**, 43–67 (2014).
- ²H. Zhu and F. Semperlotti, "Metamaterial based embedded acoustic filters for structural applications," AIP Adv. 3, 092121 (2013).
- ³A. De Sabata, L. Matekovits, A. Buta, G. Dassano, and A. Silaghi, "Frequency selective surface for ultra-wide band filtering and shielding," Sensors 22(5), 1896 (2022).
- ⁴S. G. Konarski and C. J. Naify, "Elastic bandgap widening and switching via spatially varying materials and buckling instabilities," JASA Express Lett. 1, 015602 (2021).
- ⁵F. C. Seman, R. Cahill, V. F. Fusco, and G. Goussetis, "Design of a Salisbury screen absorber using frequency selective surfaces to improve bandwidth and angular stability performance," IET Microwave Antennas Propag. 5, 149–156 (2011).
- ⁶A. Dell, A. Krynkin, K. V. Horoshenkov, and G. Sailor, "Low frequency attenuation of acoustic waves in a perforated pipe," J. Acoust. Soc. Am. **153**, 1791–1801 (2023).
- ⁷H. Dong, C. Shen, S. D. Zhao, W. Qiu, H. Zheng, C. Zhang, S. Cummer, Y.-S. Wang, D. Fang, and L. Cheng, "Achromatic metasurfaces by dispersion customization for ultra-broadband acoustic beam engineering," Nat. Sci. Rev. 9, nwac030 (2022).
- ⁸K. B. Woo and K. Jaehwan, "Frequency selective surface based passive wireless sensor for structural health monitoring," Smart Mater. Struct. 22, 025002 (2013).
- ⁹R. Gorgin, Y. Luo, and Z. Wu, "Environmental and operational conditions effects on Lamb wave based structural health monitoring systems: A review," Ultrasonics **105**, 106114 (2020).
- ¹⁰L. Zhao, J. Yang, K. Wang, and F. Semperlotti, "An application of impediography to the high sensitivity and high-resolution identification of structural damage," Smart Mater. Struct. 24, 065044 (2015).
- ¹¹J. Santini, C. Sugino, E. Riva, and A. Erturk, "Harnessing rainbow trapping via hybrid electromechanical metasurfaces for enhanced energy harvesting and vibration attenuation," J. Appl. Phys. 132, 064903 (2022).
- ¹²Z. Xu, J. Shi, R. J. Davis, X. Yin, and D. F. Sievenpiper, "Rainbow trapping with long oscillation lifetimes in gradient magnetoinductive metasurfaces," Phys. Rev. Appl. 12, 024043 (2019).
- ¹³N. K. Zanjani, M. Shayegannia, R. Prinja, A. O. Montazeri, A. Mohammadzadeh, K. Dixon, S. Zhu, P. R. Selvaganapathy, A. Zavodni, N. Matsuura, and N. P. Kherani, "Multiwavelength surface-enhanced Raman spectroscopy using rainbow trapping in width-graded plasmonic gratings," Adv. Opt. Mater. 6, 1701136 (2018).
- ¹⁴J. M. De Ponti, A. Colombi, E. Riva, R. Ardito, F. Braghin, A. Corigliano, and R. V. Craster, "Experimental investigation of amplification, via a mechanical delay-line, in a rainbow-based metasurface for energy harvesting," Appl. Phys. Lett. 117, 143902 (2020).
- ¹⁵G. J. Chaplain, D. Pajer, J. M. De Ponti, and R. V. Craster, "Delineating rainbow reflection and trapping with applications for energy harvesting," New J. Phys. 22, 063024 (2020).

- ¹⁶H. Meng, D. Chronopoulos, N. Bailey, and L. Wang, "Investigation of 2D rainbow metamaterials for broadband vibration attenuation," Materials 13, 5225 (2020).
- ¹⁷D. Zhao, Y. Li, and X. Zhu, "Broadband Lamb wave trapping in cellular metamaterial plates with multiple local resonances," Sci. Rep. 5, 9376 (2015).
- ¹⁸K. L. Tsakmakidis, A. D. Boardman, and O. Hess, "Trapped rainbow storage of light in metamaterials," Nature 450, 397–401 (2007).
- ¹⁹Q. Gan, Y. J. Ding, and F. J. Bartoli, "Rainbow trapping and releasing at telecommunication wavelengths," Phys. Rev. Lett. 102, 056801 (2009).
- ²⁰C. R. Williams, S. R. Andrews, S. A. Maier, A. I. Fernández, L. Moreno, and F. G. Vidal, "Highly confined guiding of terahertz surface plasmon polaritons on structured metal surfaces," Nat. Photonics 2, 175 (2008).
- ²¹M. S. Jang and H. Atwater, "Plasmonic rainbow trapping structures for light localization and spectrum splitting," Phys. Rev. Lett. 107, 207401 (2011)
- ²²M. A. Kats, D. Woolf, R. Blanchard, N. Yu, and F. Capasso, "Spoof plasmon analogue of metal-insulator-metal waveguides," Opt. Express 19, 14860–14870 (2011).
- ²³F. Xia, L. Sekaric, and Y. Vlasov, "Ultracompact optical buffers on a silicon chip," Nat. Photonics 1, 65–71 (2007).
- ²⁴M. F. Yanik and S. Fan, "Dynamic photon storage," Nat. Phys. 3, 372–374 (2007).
- ²⁵S. Noda, A. Chutinan, and M. Imada, "Trapping and emission of photons by a single defect in a photonic bandgap structure," Nature 407, 608–610 (2000).
- ²⁶J. Zhu, Y. Chen, X. Zhu, F. J. Vidal, X. Yin, W. Zhang, and X. Zhang, "Acoustic rainbow trapping," Sci. Rep. 3, 1728 (2013).
- ²⁷X. Ni, Y. Wu, Z. Chen, Y. Xu, P. Nayar, X. Liu, M. Lu, and Y. F. Chen, "Acoustic rainbow trapping by coiling up space," Sci. Rep. 4, 7038 (2014).
- ²⁸Z. Tian and L. Yu, "Rainbow trapping of ultrasonic guided waves in chirped phononic crystal plates," Sci. Rep. 7, 40004 (2017).
- ²⁹A. Arreola-Lucas, G. Báez, F. Cervera, A. Climente, R. A. Méndez-Sánchez, and J. Sánchez-Dehesa, "Experimental evidence of rainbow trapping and Bloch oscillations of torsional waves in chirped metallic beams," Sci. Rep. 9, 1860 (2019).
- ³⁰Y. Jin, B. Rouhani, and D. Torrent, "Gradient index phononic crystals and metamaterials," Nanophotonics 8, 685–701 (2019).
- ³¹C. Zhou, B. Yuan, Y. Cheng, and X. Liu, "Precise rainbow trapping for low-frequency acoustic waves with micro Mie resonance-based structures," Appl. Phys. Lett. 108, 063501 (2016).
- ³²L. Zhao and S. Zhou, "Compact acoustic rainbow trapping in a bioinspired spiral array of graded locally resonant metamaterials," Sensors 19, 788 (2019).
- ³³J. M. De Ponti, L. Iorio, E. Riva, R. Ardito, F. Braghin, and A. Corigliano, "Selective mode conversion and rainbow trapping via graded elastic waveguides," Phys. Rev. Appl. 16, 034028 (2021).
- ³⁴M. Alshaqaq, S. Sugino, and A. Erturk, "Programmable rainbow trapping and band-gap enhancement via spatial group-velocity tailoring in elastic metamaterials," Phys. Rev. Appl. 17, L021003 (2022).
- ³⁵G. J. Chaplain, J. M. De Ponti, G. Aguzzi, A. Colombi, and R. V. Craster, "Topological rainbow trapping for elastic energy harvesting in graded Su-Schrieffer-Heeger systems," Phys. Rev. Appl. 14, 054035 (2020).
- ³⁶X. L. Tang, T. X. Ma, and Y. S. Wang, "Topological rainbow trapping and acoustic energy amplification in two-dimensional gradient phononic crystals," Appl. Phys. Lett. 122, 112201 (2023).
- ³⁷Z. Tian, C. Shen, J. Li, E. Reit, H. Bachman, J. Socolar, and S. A. Cummer, "Dispersion tuning and route reconfiguration of acoustic waves in valley topological phononic crystals," Nat. Commun. 11, 762 (2020).
- ³⁸Q. Gan, Y. Gao, and K. Wagner, "Experimental verification of the rain-bow trapping effect in adiabatic plasmonic gratings," Proc. Natl. Acad. Sci. U.S.A. 108(13), 5169–5173 (2011).
- ³⁹V. J. Sánchez-Morcillo, K. Staliunas, and V. Romero-García, "Enhancement of sound by soft reflections in exponentially chirped crystals," AIP Adv. 4, 124402 (2014).
- ⁴⁰L. G. Bennetts, M. A. Peter, and R. V. Craster, "Graded resonator arrays for spatial frequency separation and amplification of water waves," J. Fluid Mech. 854, R4 (2018).
- ⁴¹A. J. Archer, H. A. Wolgamot, J. Orszaghova, L. G. Bennetts, M. A. Peter, and R. V. Craster, "Experimental realization of broadband control of water-wave-energy amplification in chirped arrays," Phys. Rev. Fluids 5, 062801(R) (2020).

https://doi.org/10.1121/10.0025179

JASA

- ⁴²E. A. Skelton, R. V. Craster, A. Colombi, and D. J. Colquitt, "The multiphysics metawedge: Graded arrays on fluid-loaded elastic plates and the mechanical analogues of rainbow trapping and mode conversion," New J. Phys. 20, 053017 (2018).
- ⁴³I. Arretche and K. H. Matlack, "Effective phononic crystals for non-Cartesian elastic wave propagation," Phys. Rev. B 102, 134308 (2020).
- ⁴⁴I. Arretche and K. H. Matlack, "Locally resonant effective phononic crystals for subwavelength vibration control of torsional cylindrical waves," J. Vib. Acoust. **144**(3), 031007 (2022).
- ⁴⁵A. Hvatov and S. Sorokin, "On application of the Floquet theory for radially periodic membranes and plates," J. Sound Vib. 414, 15–30 (2018).
- ⁴⁶E. Manconi, A. Hvatov, and S. V. Sorokin, "Numerical analysis of vibration attenuation and bandgaps in radially periodic plates," J. Vib. Eng. Tech. 11, 2523–3939 (2023).
- ⁴⁷E. Faccioli, F. Maggio, R. Paolucci, and A. Quarteroni, "2D and 3D elastic wave propagation by a pseudo-spectral domain decomposition method," J. Seismol. 1, 237–251 (1997).
- ⁴⁸M. A. Attarzadeh and M. Nouh, "Non-reciprocal elastic wave propagation in 2D phononic membranes with spatiotemporally varying material properties," J. Sound Vib. 422, 264–277 (2018).
- ⁴⁹P. Liu, Z. Tian, K. Yang, T. Naquin, N. Hao, H. Huang, J. Chen, Q. Ma, H. Bachman, and T. Huang, "Acoustofluidic black holes for multifunctional in-droplet particle manipulation," Sci. Adv. 8, 2592 (2022).